Observer for thick layer of solid Deuterium-Tritium using backlit optical shadowgraphy and interferometry

Alexandre Choux[★✠], Eric Busvelle[✠], Jean Paul Gauthier[✠], Ghislain Pascal[★]
[★]CEA Valduc, DRMN/SMCI/L2C,
21 120 Is sur Tille, France
[✠]Université de Bourgogne, Le2i, UMR CNRS 5158,
9 avenue Alain Savary, 21 000 Dijon, France
alexandre.choux@cea.fr, alexandre.choux@caramail.com
busvelle@u-bourgogne.fr
gauthier@u-bourgogne.fr
ghislain.pascal@cea.fr

May 4, 2007

Abstract

This paper is in the context of the French "laser mégajoule" project, about fusion by inertial confinement. The project leads to the problem of characterizing the inner surface of the approximately spherical target, by optical shadowgraphy techniques.

The paper is entirely based on the basic idea that optical shadowgraphy produces "caustics" of systems of optical rays, that contain a lot of 3D information about the surface to be characterized.

We develop a method of 3D reconstruction based upon this idea plus a "small perturbations" technique.

Although computations are made in the special "spherical" case, the method is in fact general and may be extended to several other situations.

List of Figures

1	The building with the 10m diameter shooting sphere	2
2	The LMJ target	3
3	The microshell inside the cylindrical cavity.	4
4	Infrared heating of the target	5
5	A visible first bright ring	8
6	Some optical paths.	9
7	Definitions of ρ, u and $R_u(\rho)$.	10
8	A radial profile	12
9	Concentration of rays around the caustic.	13
10	Superposition of the detected caustic	15
11	A reconstructed deformation	21
12	Comparison between cuts of original and reconstructed surfaces	22

Keywords : cryogenic microshells, shadowgraphy, caustics, data reconciliation, 3D reconstruction.

1 INTRODUCTION

1.1 The laser mégajoule project

The Laser-Mégajoule project (LMJ) is the french project of CEA ("commissariat à l'énergie atomique") on inertial confinement fusion [9]. The thermonuclear fusion or ignition shall be obtained by the implosion of solid deuterium-tritium (DT) fuel layer inside a polymer spherical shell. This cryogenic target is a 100 μm thick layer of solid deuterium-tritium at 18.2K uniformly distributed around the inner surface of a 175 μm thick spherical polymer shell with diameter 2430 μm. This one is located at the center of a cylindrical hollow cavity.

In order to achieve ignition by inertial confinement fusion, the physicist's requirements, that are due to theoretical modeling, for DT-layer thickness and "roughness"[1] are extremely stringent (on shadowgraphic images, the "roughness" must be less than 1 μm [6] and the accuracy on the thickness less than 1 μm). If the DT layer is perturbed by any thermal effect, or if the roughness is too important, some hydrodynamics instabilities could happen

[1]The "roughness" along an equator is, following the CEA, the fraction of the total energy corresponding to harmonics of order ≥ 2.

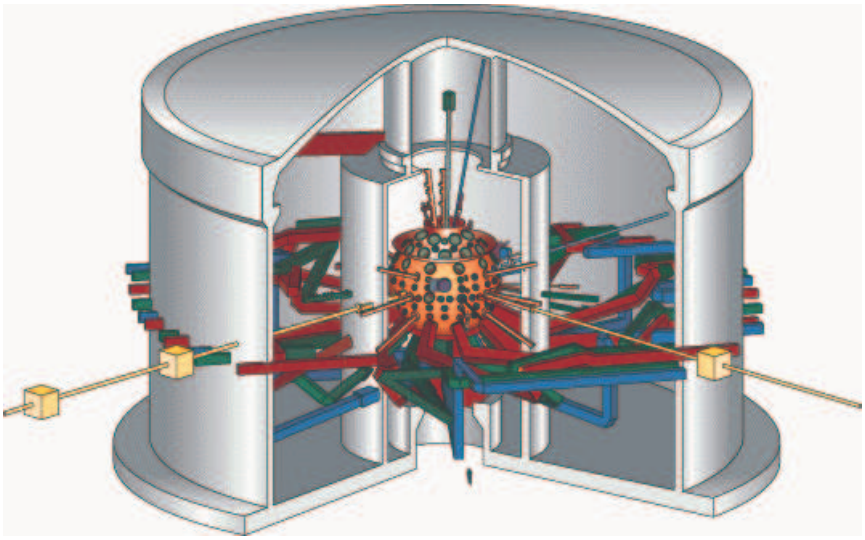

Figure 1: The building with the 10m diameter shooting sphere

during the implosion. This target will be positioned to be shot by the laser only when the specification of the roughness and the homogeneity of the layer will be obtained.

For these reasons, there is a preliminary **conformation** step of the DT-layer. This conformation step is the subject of our work.

1.2 The conformation step

The ice layer is approximately conformed by natural self heating due to the radioactive decay of tritium, called β-layering. The DT sublimates from the thicker parts of the layer and recrystallizes and deposits on the thinner parts of the layer. More details about the β-layering process can found in [8] and [11].

The final conformation of the DT-layer will be performed by the control of the thermal environment of the shell.

Since the high frequency perturbations of the DT-layer will be rubbed out by the β-layering phenomenon, it is expected that the remaining long-term perturbations of the DT-layer will have mostly two causes:

- The effect of gravity,
- The holes located at the top and bottom of the cylindrical cavity.

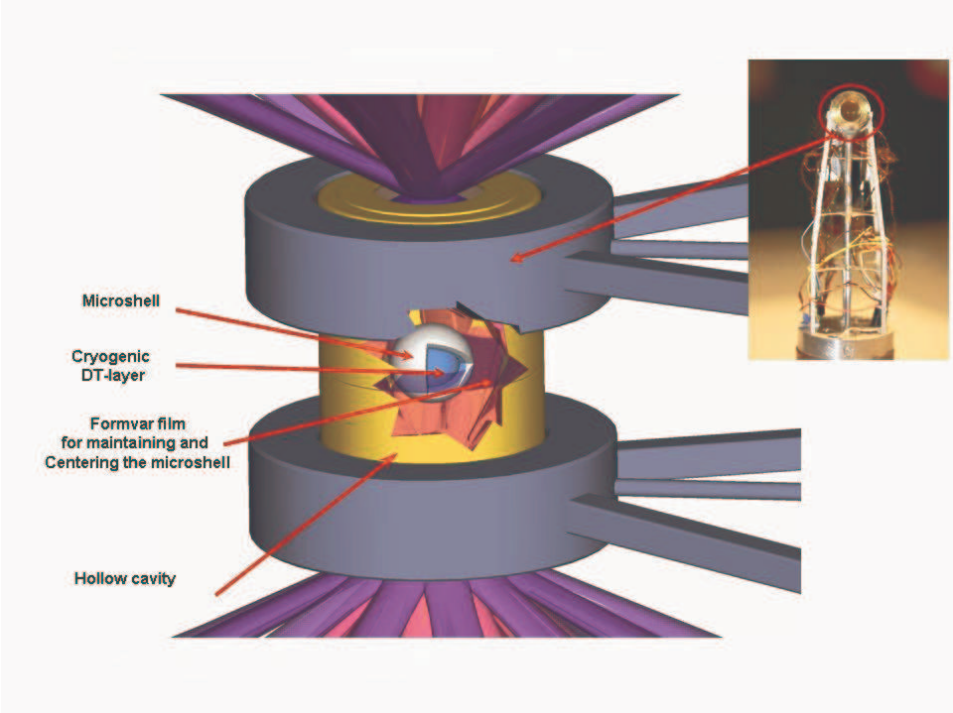

Figure 2: The LMJ target

In both cases, expected perturbations will keep the actual symmetry of the cylindrical cavity. Certainly the long-term shape of the DT-layer looks a "pear" as in Figure 11.

The role of the conformation step is to correct the effect of the perturbations. To do this, as in any control problem, we need:

1. Some control inputs,

2. Enough measurements of the shape of the DT-layer.

The possible control inputs are of two types: a) thermal resistors dispatched around the cylindrical cavity, b) infrared lasers heating the target as shown on Figure 4.

As in any control problem, the point 2. above is **crucial**. In fact, we have rather few available measurements of the DT-layer in our system. This is due to the fact that measurements can be performed through the holes of the cylindrical cavity. This is the major constraint that restricts the possibility to get informations on the thickness of the solid DT layer.

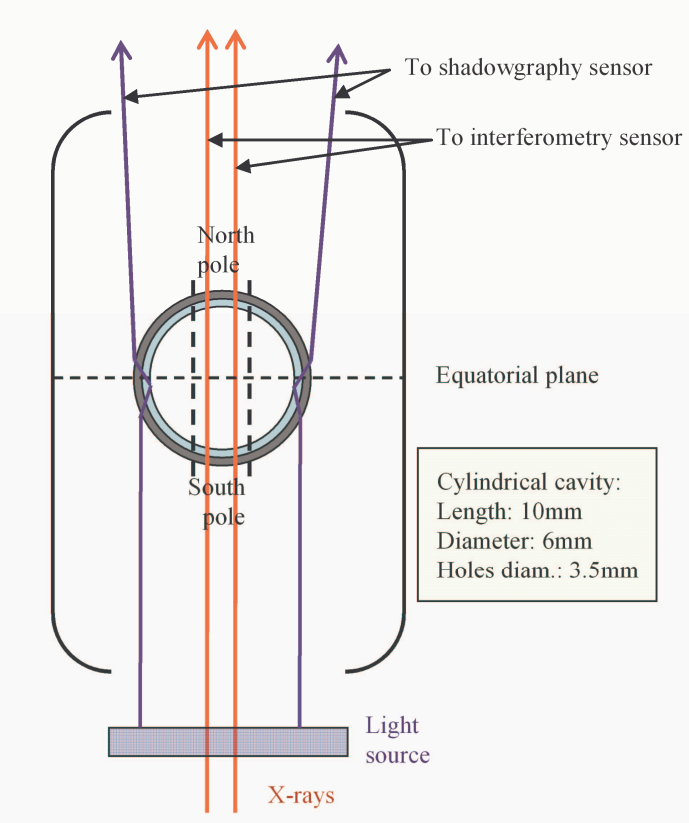

Figure 3: The microshell inside the cylindrical cavity.

As depicted on Figure 3, we have two types of measurements: a) interferometric measurements providing direct estimation of the thickness in neighbourhoods of the poles, b) backlit optical shadowgraphy, that will provide information around the equator of the microshell perpendicular to the symmetry axis.

1.3 The goals of the paper

This paper deals only with the observation process, i.e. the 3D reconstruction of the inner surface of the DT-layer from the interferometric and shadowgraphic data. The control part of the problem (we are working on it now) will be treated by very classical control methods, about which we don't give any detail here. This choice of classical methods is justified partly by the fact that the system is dynamically first order, the time constant of the β-layering phenomenon being about 20 minutes.

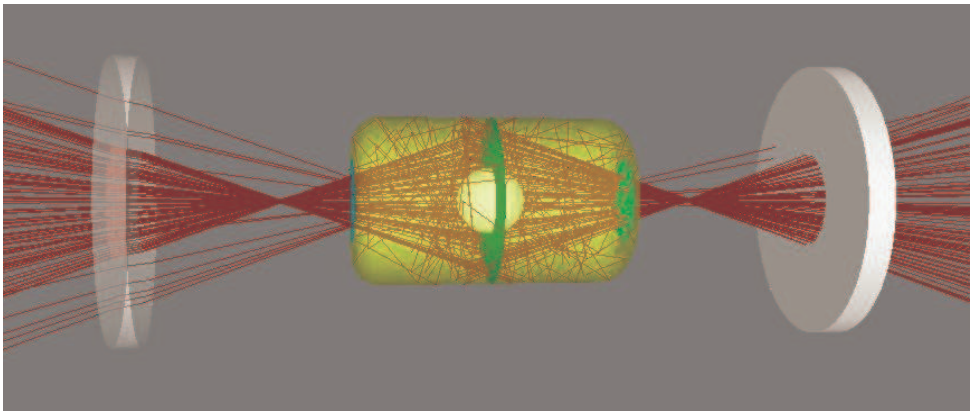

Figure 4: Infrared heating of the target

To perform the 3D reconstruction, at some step we will reconcile the shadowgraphic data with the direct interferometric measurements. This reconciliation will be done via a standard least-square procedure. Moreover, we don't have yet any practical interferometric measurements. It is why **the paper focusses on the use of shadowgraphic measurements** for 3D reconstruction.

Actually, the shadowgraphic information is concentrated in a mathematical object called a "**caustic**". It is the envelope of a system of optical rays (described precisely later). The intersection of this caustic (which is a surface in the space $\mathbb{R}^3$) with the plane of the optical sensor gives rise to a certain "bright ring" as shown on Figure 5. Together with the interferometric measurement (localized at the poles), this bright ring is the only information we have to perform the 3D reconstruction.

There are three keypoints guiding us in our analysis of the shadowgraphic data:

1. The bright ring is a one dimensional object, but as a piece of a caustic, **it contains some 3D information** that we have to use in an optimal way,

2. Due to the symmetries of the problem, the ideal situation (a perfectly spherical DT-layer) where we want to go, can be computed explicitly (it is elementary but tedious),

3. The practical situation (the perturbed DT-layer) can be studied by a technique of **small perturbation** of the ideal situation.

At this point, some comments are absolutely necessary.

For point 1., the caustic (which is mathematically **a singularity of the system of rays**) contains a lot of information about the system of rays itself. It is a common idea from singularity theory that singularities determine everything ([1]). Hence the caustic should reflect the optical properties i.e. the Descartes laws that express that the rays are reflected or refracted with respect to the normal to the DT-surface. Then the bright ring certainly contains informations about **the position** of the DT-surface, but also about its normal or equivalently **its tangent plane**.

Concerning point 3., it should be noticed that many complications appear in small perturbation techniques when **perturbing singularities**. But this is exactly our case. Moreover, our caustic is in fact a "Lagrangian[2] singularity" (in the sense of Arnold [1]). In fact, our problem is a problem of **perturbation of Lagrangian singularities**. Because of this, it is mathematically delicate.

Our methodology goes far beyond the scope of this paper: **it is in fact very general** and it could be applied to many other situations in optical shadowgraphy, where we have a perturbation of some ideal very[3] symmetric situation.

To our knowledge, there are two papers in the litterature that are closely related to our work: [3, 12]. The contributions of the paper [3] are explained inside this paper. The paper [12], still unpublished, mostly establishes paralelly to us the formulas of the ideal unperturbed caustic in Section 2.3.

1.4 Contents of the paper

The paper is organized as follows:

- In section 2, the principles of the backlit optical shadowgraphy is recalled. We observe the appearance of a series of bright rings (caustics) corresponding to several types of optical paths. In the paper, we focus on the main bright ring only (the others having a less significant energy). We establish the equation of this ring in the ideal case of a perfectly spherical and centered DT-layer.

- Section 3 is devoted to the extraction from the picture of the piece of the caustic contained in the sensor plane.

[2]In Lagrangian singularity theory, some quantity has to be minimized. Here, it is the length of the optical paths.

[3]Mathematically, we mean a situation whith a large symmetry group.

- In Section 4, we establish our main formula (9) for the perturbed caustic. Let A be a point on the (previously extracted) bright ring. It corresponds to a point P on the inner DT-surface. The angle between the normal at P to the surface and the symmetry axis is called ω. Our formula relates **at first order** the quantities A, P and ω.

- In the next section 5, we treat our data reconciliation problem. The perturbed DT-surface is described by a certain linear combination of spherical harmonics. But our problem is in fact ill-posed: it is even intuitively clear, due to the geometry, that our system is unobservable[4] (with respect to the shadowgraphic data only). We overcome this difficulty in the following way.

1. We make some a-priori choice of the relevant spherical harmonics, that are related to the nature of the expected perturbations (see Section 1.2).

2. We use the shadowgraphic data to identify the observable components only.

3. Some unobservable components will be completely determined by the interferometric data.

In fact, these three points will be used inside a unique least-square procedure.

- Finally, Section 6 delivers our short conclusions.

2 SHADOWGRAPHY AND IDEAL CAUSTIC

2.1 Preliminary

The backlit optical shadowgraphy is a technique which consists of putting the studied object between a light source and a camera. The monochromatic collimated light crosses the cavity along its radial axis and reaches the sensor plane of the camera (Figure 3). The pictures that are obtained show the shadow of the lighted object, as we can see on the Figure 5.

[4]This concept will be explained precisely later. It means that there is not enough information in the shadowgraphic data to reconstruct the full inner surface.

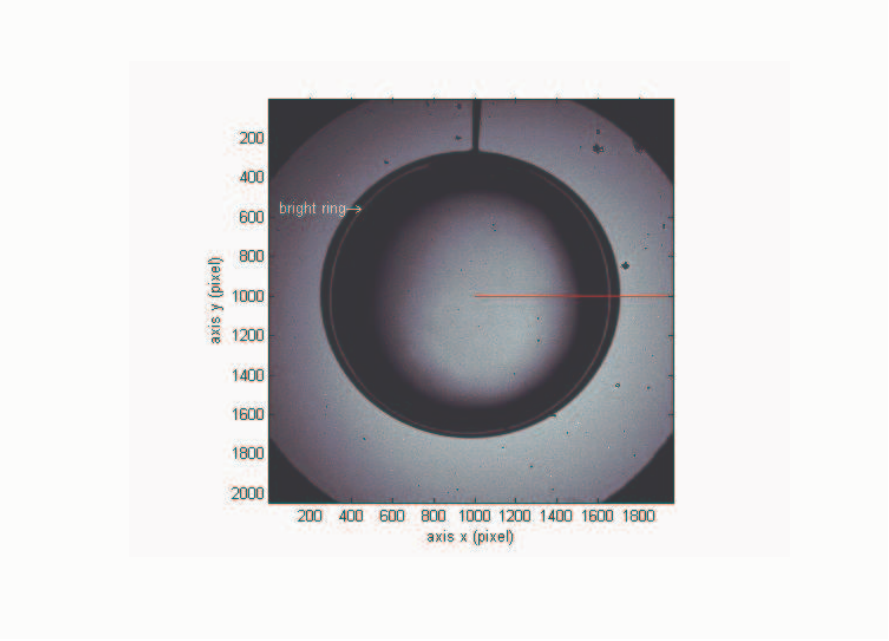

Figure 5: A visible first bright ring

Due to permeability to light, with different refraction indices, of both the spherical shell and the DT-layer, a single light ray from the source gives rise to several optical paths, with different energy. This is depicted on Figure 6 (b), (c). We are concerned with optical paths of type (b) only. The figure 6 (a) illustrates the relative dimensions of the different pieces of the full optical device, including the CCD sensor, from which our images come.

The studied target is a hydrocarbon polymer microshell (with refractive index 1.54) that contains a solid layer of deuterium-tritium (with refractive index 1.16). The distance between the center of the microshell and the lens of the camera is twice the focal of the lens, denoted by f $(f = 197.5mm)$. The device has a **vertical** axial symmetry (**the optical axis**). The CCD sensor is 1964×2048 pixels. The size of the pixels is $6 * 6\,\mu$m. The numerical aperture of the lens is 0.084 and the magnitude we get is -3 (It is not -1 as expected, because of another lens at the level of the camera). To observe the shadowgraphic pictures, the light source before the collimator consists of a lamp with green-filtered monochromatic spectrum that has no effect on the temperature distribution of the target.

On Figure 6 (b), the optical paths that will be considered in the shadowgraphy system go from the left to the right. The rays of Figure 6 (a) on the right, after crossing the lens determine a caustic (their envelope). The

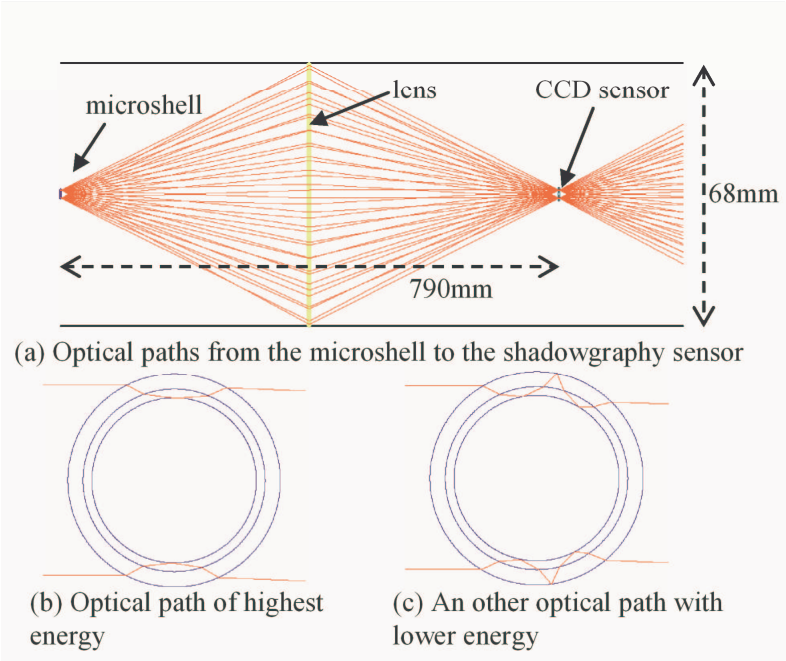

Figure 6: Some optical paths.

intersection of this caustic with the sensor plane is the bright ring on Figure 5.

As explained before, we exploit only the (perturbed) main ring, i.e. the one with maximum energy. The (ideal) corresponding ring is a perfect circle due to the cylindrical symmetry of the system around the optical axis.

2.2 Computation of the ideal optical path

We compute the equation of the **ideal paths** first. In the notations, to distinguish this ideal spherical case from the general perturbed case, we use the superscript $*$. For instance if r denotes a radius in the perturbed case, r^* denotes the radius in the ideal case.

Due to the cylindrical symmetry, it is clear that calculations may be done in any plane containing the optical axis (all ideal optical paths stay in such planes). We chose one denoted by $\mathcal{P}$. The orthonormal coordinate system (ρ, u) in the plane $\mathcal{P}$ is centered at the point located along the optical axis at distance $4f$ of the center of the microshell, u being the coordinate along the optical axis.

We consider a ray $\mathcal{R}$ in $\mathcal{P}$ issued from the source at ρ coordinate equal

to ρ_0. The unique point on this ray $\mathcal{R}$ with u-coordinate equal to u_0 has a ρ-coordinate denoted by $R^*_{u_0}(\rho_0)$. This is illustrated on Figure 7.

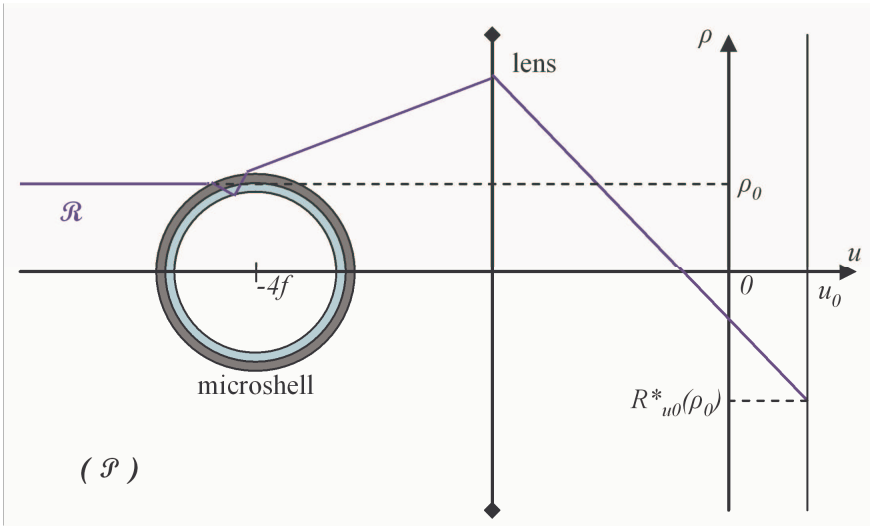

Figure 7: Definitions of ρ, u and $R_u(\rho)$.

Note that to compute $R^*_u(\rho)$ as a function of u and ρ, we just need to know the Descartes refraction and reflection laws.

The map $R^*_u(\rho)$ has the following form:

$$R^*_u(\rho) = h_1(\rho) + u\, h_2(\rho),$$

were $h_1(\rho)$ and $h_2(\rho)$ are smooth functions with respect to the variable ρ, depending on the optical system only. They are computed as a composition of several maps corresponding to the different refraction and reflection steps of the path under consideration, and are given by:

$$h_1(\rho) = \frac{\rho}{\cos 2\Psi} \tag{1}$$

$$h_2(\rho) = \frac{1}{f} h_1(\rho) + \tan 2\Psi \tag{2}$$

with,

$$\begin{aligned}\Psi = \arcsin\frac{\rho}{r_{ext}} - \arcsin\frac{n_{ext}\rho}{n_{\mu b} r_{ext}} + \arcsin\frac{n_{ext}\rho}{n_{\mu b} r_{int}} \\ - \arcsin\frac{n_{ext}\rho}{n_{DT} r_{int}} + \arcsin\frac{n_{ext}\rho}{n_{DT} r_{DT}}\end{aligned} \tag{3}$$

where n_{ext}, $n_{\mu b}$ and n_{DT} are respectively optical indices of exterior environment, microshell and DT; r_{ext} and r_{int} are external and internal radius of the microshell, and r_{DT} is the radius of the DT-layer.

2.3 Computation of the ideal caustic and the ideal ring

Then, the caustic, which is the envelope of our system of rays coincides with the set of singular values of the "suspended" mapping $\mathcal{S}$:

$$\mathcal{S} : (\rho, u) \longrightarrow (R_u^* (\rho), u).$$

It means that the caustic will be defined by the equation,

$$\frac{\partial R_u^* (\rho)}{\partial \rho} = 0.$$

Given a u, this equation has a single solution obtained at $\rho^* (u)$. The ideal caustic keeps the cylindrical symmetry of the ideal case. It is parametrized by u and any point on the caustic has coordinates $(R_u^* (\rho^* (u)), u) := (R_u^*, u)$.

Observe that, if we set $u = 0$, the u-coordinate of the sensor plane, we get the equation of the ideal ring:

$$\frac{\partial R_0^*}{\partial \rho} = 0. \tag{4}$$

Then, the radius of the (ideal) bright ring in the u-plane is $(u = 0)$

$$R_c^* = h_1 (\rho^*).$$

Remark 1 *It results from this characterization that the ray corresponding to the caustic i.e. the ray starting from the source at ρ^* does not touch the inner DT-surface at the equator but a bit before (about 2 degrees). Then, even in the ideal spherical case, the bright ring is not exactly an image of the "great circle".*

Since we consider a single type of optical path, the energy of each ray is the same. Hence there is an irradiance map, giving the lighting of the plane-optical-sensor. Along a radial ray in the sensor plane (Figure 5), we get an intensity profile, cf Figure 8.

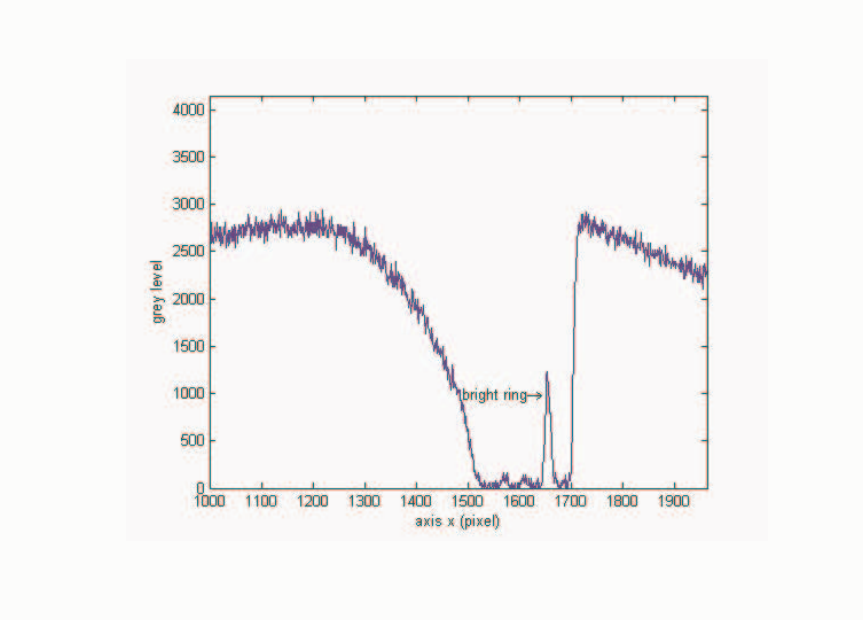

Figure 8: A radial profile

Remark 2 *Note that on this intensity profile (Figure 8), the jump on the right side corresponds to the exterior boundary of the microshell, although the peak corresponds to the bright ring. Due to the mathematical fact that the bright ring is the trace of a caustic, the exact position of this trace corresponds to the left (inner) part of the peak (which is more vertical than the right (outer) part as observed on the figure 8). This property is due to the fact that the caustic is an envelope, and can be understood on the figure 9 describing the system of rays in a neighbourhood of the caustic.*

Hence, isolating the caustic is equivalent to detecting the left (inner) part of this peak.

We will crucially use the following: **this remark is still true in the perturbed case**.

3 BRIGHT RING ANALYSIS

As usual in "technical characterization" of materials, when it is difficult to relate directly the observations made to the physical properties of the object to be characterized, engineers use to make "normalized trials". In this spirit,

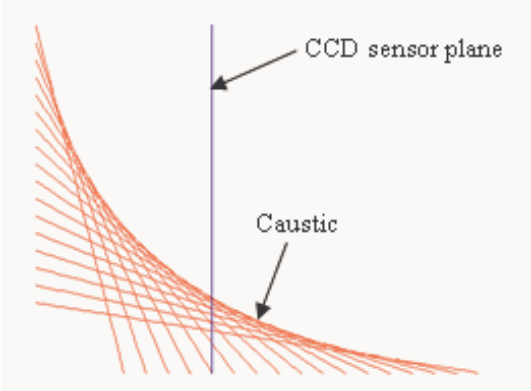

Figure 9: Concentration of rays around the caustic.

the engineers at CEA (french "commissariat à l'énergie atomique") defined the "2D-roughness" of the inner DT-surface along some equator as follows: The bright ring being described in polar coordinates as a function $R(\theta)$, the 2D-roughness is the fraction of the power spectral density of the Fourier series expansion of $R(\theta)$ corresponding to high harmonics.

Behind this "normalized trial" notion of 2D-roughness, there is the idea that the bright ring provides, just after rescaling, a perfect image of the inner DT-surface along the equator. As we have pointed out in the previous section (Remark 1), **this is not true**. Nevertheless, this assumption is made in the paper [3].

In the same spirit, the 3D-roughness[5] of the DT-surface $\mathcal{S}(\theta, \varphi)$ expressed in polar coordinates can be defined as a fraction of power spectral density corresponding to spherical harmonics of order ≥ 2 (spherical harmonics of order 1 are just related to eccentricity).

We have to perform some image analysis: from the picture in the sensor-plane, we have to extract the main bright ring. The purpose of this extraction is twofold:

- First, perform on it standard Fourier analysis to compute the value of the 2D-roughness along the equator.
- Second, with the results of the next paragraph, using the bright ring, we will reconstruct precise information about the inner surface of the DT-layer, including its tangent plane along a closed curve (lying on the inner DT surface) near the equator plane.

[5] A better terminology would be the "default of sphericity" of the target.

Due to the Remark 2, a standard zero-crossing technique can be used to detect precisely the trace of the caustic on the sensor plane. We use the very classical "Laplacian edge detection" method of [10], because of its invariance with respect to 2D–rotations-translations. This isotropy property is crucial in our case: a method polarized in the direction of the coordinates axes (e.g. Sobel method or other) would produce artificial modes of order 4, 8, and so on.

Therefore, to extract the bright ring, we proceed as follows:

Starting from the outer board of the microshell, we encounter a certain number of zeros of the laplacian: the first one corresponds to the shell, the second one to the outer smooth board of the concentration of rays close to the caustic, the third one corresponds to the vertical jump of the caustic, the other zeros correspond to other caustics from different optical paths. Hence we have to detect the third zero crossing.

This set of points is unfolded in polar coordinates. Thereafter the points are approximated–interpolated with C^2–splines on the circle using the least square method (it happens that there are large holes on the bright ring, presumably due to non–C^1 perturbations of the surface).

Fourier analysis of this approximation provides the 2D–roughness. Moreover, the resulting approximation will be used in the next sections for the global reconstruction of the inner shape of the DT-layer.

This method has been compared to another one, developed at University of Rochester (see [3]), with positive conclusion.

Figure 10 shows the superposition of the reconstructed caustic (its intersection with the sensor plane) and the image.

With this global zero-crossing technique, we reach the accuracy of 0.1 pixel approximately.

4 SHADOWGRAPHIC ANALYSIS

In this section, which contains our most important theoretical results, **we give only the main ideas of computations and proofs**. Detailed proofs are given in the Ph.D. thesis [2]. Our purpose is to relate (at order 1) the extracted piece of the caustic to the inner surface of the DT layer.

The solid DT layer is a perturbation of the ideal one. Consequently the main ideal bright ring will be disturbed. Disturbances of the inner surface are modelled by a perturbation ε_1 of the radius of the inner sphere, and a

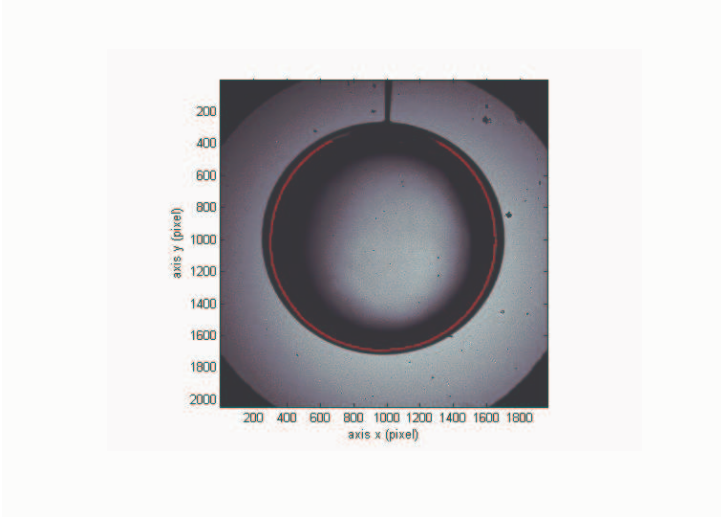

Figure 10: Superposition of the detected caustic

perturbation ε_N of the ideal unit normal vector U. These perturbations ε_1, ε_N are assumed to be smooth and small in the C^1 sense.

At the point p under consideration on the inner (ideal) sphere we have (modulo orientation) an (ideal) orthonormal frame (U, V, W), where V is contained in the plane defined by p and the optical axis. The perturbation ε_N expressed in this frame has components $\sqrt{1-\varepsilon_2^2-\varepsilon_3^2}$, ε_2, ε_3 in the directions of U, V, W respectively. Let ω_2 be the angle between U and ε_N. Since at first order, $\sin(\omega_2) \simeq \omega_2$, ε_2 can be identified to this angle ω_2.

In the following, the notation O^i refers to expressions of order[6] i in ε_1 ,ε_2 ,ε_3 and their first derivatives.

Remark 3 *Note that these three perturbations are not independent. This fact has no consequence in the theoretical results in this section. But, it will be implicitly taken into account when we will merge the whole data by a least square method. Since the ε_i's are not independent, the C^1 assumption correspond to* ***the assumption of a small C^2 perturbation of the inner surface of the DT-layer****. Hence, ε_1 has in fact to be assumed C^2-small for ε_2, ε_3 be C^1-small.*

Now in the perturbed case, it is no longer possible to assume that the full paths stays in a plane (containing the optical axis). Hence we have to parametrize our problem in $\mathbb{R}^3$.

[6]Here a function of ε_1 ,ε_2 ,ε_3 has order i if it belongs to the i^{th} power of the ideal generated by ε_1, ε_2, ε_3.

Let $\rho \in \mathbb{R}$ and $\theta \in [0, 2\pi[$ be the polar coordinates of a starting collimated light ray in a plane perpendicular to the optical axis.

Let $R \in \mathbb{R}$ and $\alpha \in [0, 2\pi[$ be the polar coordinates of the intersection of this light ray with the optical sensor (in its own plane).

As above, let $R_0^*(\rho)$ denote the distance to the origin of the intersection point of a ray (starting with coordinate ρ) with the sensor-plane $u = 0$, in the ideal unperturbed situation.

The following theorem is a consequence of both the axial symmetry of the ideal situation and the required smoothness of the perturbation. The proof is just writing explicitly the expansion of the successive refractions and reflections. It is a straightforward but tedious computation. It has been checked by using Mathematica.

Theorem 4

$$R(\rho, \theta) = R^*(\rho) + a_1(\rho)\varepsilon_1(\rho, \theta) + a_2(\rho)\varepsilon_2(\rho, \theta) + O^2, \tag{5}$$

$$\alpha(\rho, \theta) = \theta + a_3(\rho)\varepsilon_3(\rho, \theta) + O^2, \tag{6}$$

for certain smooth real functions a_1,a_2,a_3.

Note that the functions a_1, a_2, a_3 depend only on the properties of the optical system. They are complicated trigonometric functions that we don't show here.

For the same reasons (symmetry of the ideal situation, and smoothness of the perturbations), the following theorem is easily proved:

Theorem 5 *The equation of the caustic is still given by:*

$$\frac{\partial R}{\partial \rho}(\rho, \theta) = 0.$$

The implicit function theorem shows that we can solve equation (6) in order to get:

$$\theta(\rho, \alpha) = \alpha - a_3(\rho)\varepsilon_3(\rho, \alpha) + O^2. \tag{7}$$

Then replacing (7) in (5) gives:

Theorem 6 *The equation of* R *in the coordinates* (ρ, α) *is:*

$$R(\rho, \alpha) = R^*(\rho) + a_1(\rho)\varepsilon_1(\rho, \alpha) + a_2(\rho)\varepsilon_2(\rho, \alpha) + O^2, \tag{8}$$

and the equation of the caustic is still given by $\dfrac{\partial R}{\partial \rho}(\rho, \alpha) = 0$ *in these coordinates* (ρ, α) *in place of* (ρ, θ).

Remark 7 *Let us point out that:*

1) computations to obtain the three previous theorems used explicitly the fact that we are studying perturbations of a Lagrangian singularities,

2) for the proof of theorem 6, ***the fact that we are on a point of a caustic is crucial****,*

3) the perturbation ε_3 has no effect at order 1 on the radius of the caustic.

Now, using the expansion (8) of Theorem 6, we will compute the first order expansion of the caustic of the perturbed system.

Let ρ^* denote the radial coordinate of the starting rays of the unperturbed system, intersecting the sensor plane on the ideal caustic. Let φ^* denote the corresponding angle between the line [from the center of the microshell to the contact point on the ideal DT-layer] and the optical axis.

Theorem 8 *The equation at order 1 of the perturbed caustic, in the coordinates (ρ, α) is given by:*

$$R_c(\alpha) = R^*(\rho^*) + a_1(\rho^*)\varepsilon_1(\rho^*, \alpha) + a_2(\rho^*)\varepsilon_2(\rho^*, \alpha) + O^2, \tag{9}$$

where $R_c(\alpha)$ denotes the radius in the sensor plane of the point of the caustic of angle α.

Proof. The proof again uses deeply the fact that we deal with a caustic. Let us use Theorem 6. If $\rho^* + \delta\rho$ is the radial value of ρ for the point of the inner DT-layer corresponding to the perturbed caustic, we get:

$$\begin{aligned} 0 = {} & \frac{\partial R^*}{\partial \rho}(\rho^* + \delta\rho) + \frac{\partial a_1}{\partial \rho}(\rho^* + \delta\rho)\varepsilon_1(\rho^* + \delta\rho, \alpha) + a_1(\rho^* + \delta\rho)\frac{\partial \varepsilon_1}{\partial \rho}(\rho^* + \delta\rho, \alpha) \\ & + \frac{\partial a_2}{\partial \rho}(\rho^* + \delta\rho)\varepsilon_2(\rho^* + \delta\rho, \alpha) + a_2(\rho^* + \delta\rho)\frac{\partial \varepsilon_2}{\partial \rho}(\rho^* + \delta\rho, \alpha) + O^2. \end{aligned}$$

Expanding, and using the fact that ε_1 is C^2 small and ε_2 is C^1 small, we obtain:

$$\begin{aligned} 0 = {} & \frac{\partial R^*}{\partial \rho}(\rho^*) + \delta\rho\frac{\partial^2 R^*}{\partial \rho^2}(\rho^*) + \frac{\partial a_1}{\partial \rho}(\rho^*)\varepsilon_1(\rho^*, \alpha) + a_1(\rho^*)\frac{\partial \varepsilon_1}{\partial \rho}(\rho^*, \alpha) \\ & + \frac{\partial a_2}{\partial \rho}(\rho^*)\varepsilon_2(\rho^*, \alpha) + a_2(\rho^*)\frac{\partial \varepsilon_2}{\partial \rho}(\rho^*, \alpha) + \delta\rho O^1 + O^2. \end{aligned}$$

Now, by definition of R^* and ρ^*, and by the fact that the ideal caustic is also characterized by $\frac{\partial R^*}{\partial \rho}(\rho) = 0$, we have in fact $\frac{\partial R^*}{\partial \rho}(\rho^*) = 0$.

Also, straightforward direct computations in the ideal situation show that $\frac{\partial^2 R^*}{\partial \rho^2}(\rho^*)$ is a nonzero constant. From this, we get (using the implicit function theorem) that $\delta\rho = O^1$. Replacing this relation in (8) gives:

$$R_c(\alpha) = R^*(\rho^*+O^1)+a_1(\rho^*+O^1)\varepsilon_1(\rho^*+O^1,\alpha)+a_2(\rho^*+O^1)\varepsilon_2(\rho^*+O^1,\alpha)+O^2,$$

which, at first order implies, using again that $\varepsilon_1, \varepsilon_2$ are C^1 small:

$$R_c(\alpha) = R^*(\rho^*) + \frac{\partial R^*}{\partial \rho}(\rho^*)O^1 + a_1(\rho^*)\varepsilon_1(\rho^*,\alpha) + a_2(\rho^*)\varepsilon_2(\rho^*,\alpha) + O^2.$$

This is the expected result. ■

This (affine at order 1) relation (9), using practical measurements of $R_c(\alpha)$ from Section 3 (in which the angle coordinate is α, the angle of a point of the caustic **in the sensor plane**), will allow us to recover, by a method explained in the next section, the whole information about the disturbances $\varepsilon_1(\rho^*,\alpha)$ and $\varepsilon_2(\rho^*,\alpha)$ of the ideal spherical surface.

It is also not so hard to prove that (since ε_1 is assumed C^2 small):

$$\varepsilon_3(\rho^*,\theta) = \frac{1}{R\cos^2(\varphi^*)}\frac{\partial \varepsilon_1(\varphi^*,\theta)}{\partial \theta} + O^2. \tag{10}$$

Remark 9 *Due to the relations (7, 10), if we know $\varepsilon_1(\rho^*,\alpha)$, it is possible to reconstruct $\theta(\rho^*,\alpha)$ at order 1 in terms of α (which is the angle observed in practice). In fact, it seems that this order 1 correction of the relation at order zero:*

$$\theta(\rho^*,\alpha) = \alpha + O^1, \tag{11}$$

is of no significant importance on the final results. Therefore, in the next section, for the purpose of practical reconstruction of the inner surface of the DT-layer, we will use only relation (11) in place of (10).

5 DT LAYER ESTIMATION

5.1 Modelling of the perturbed surface

Let us consider the previous angle θ together with the other angle φ, in order to form Euler-like coordinates around the center of the microshell. Then, the inner surface of the DT-layer is modelled as a perturbation $\varepsilon(\theta,\varphi)$ of the ideal spherical inner surface of the DT-layer. As we said above, this perturbation

is assumed to be C^2-small. It will be modelled a-priori as a finite sum of spherical harmonics

$$\varepsilon(\theta,\varphi) = \sum\nolimits_{i=1}^{i=k} \lambda_i . e_i(\theta,\varphi) . \tag{12}$$

where λ_i are constants and represent the magnitudes of each spherical harmonics $e_i(\theta,\varphi)$.

This is standard: disturbances of spheres are generally modelled by spherical harmonics [7], [5]. **What is not standard here is our choice of the relevant spherical harmonics** $e_i(\theta,\varphi)$. Here, we introduce **some a-priori information**. Practically, we consider only spherical harmonics that can occur in the physical configuration as explained in Section 1.2. In fact, the perturbations have three origins: 1) the gravity (the optical axis is in practice vertical), 2) the thermal disturbances coming from the two windows of the cylindrical cavity, that are located above and below the device, and 3) position errors of the centre of the microshell w.r.t. the centre of the cylindrical cavity. The third perturbation is expected to be small in the final shooting configuration. We will only keep spherical harmonics that give rise to these perturbations. Of course, we limit ourselves to spherical harmonics of low order (about 15).

Remark 10 *Note that the C^2-small disturbance $\varepsilon(\theta,\varphi)$ completely determines our perturbations $\varepsilon_1, \varepsilon_2, \varepsilon_3$ above: ε_1 is the restriction of ε to the closed curve on the DT-layer corresponding to our extracted ring.*

5.2 Observability

At this point, another important problem appears. Consider the mapping

$$\Theta : \varepsilon(\theta,\varphi) \longrightarrow \Delta R_c(\theta) = R_c(\theta) - R^*$$

where $\varepsilon(\theta,\varphi)$is the perturbation of the surface, and $R_c(\theta)$ is the corresponding intersection of the caustic with the sensor plane. We have computed this mapping at order 1 only, i.e. our approximation $A\Theta$ of the mapping Θ is linear.

It turns out that this linear mapping $A\Theta$ has a nonzero kernel K, even in restriction to the subspace $\mathcal{S}$ of spherical harmonics determined by our a-priori choices. It means that, on the basis of the shadowgraphic data, we can expect to reconstruct only the component of ε on the orthogonal complement of K in $\mathcal{S}$. This is the "**unobservability property**".

For the reconstruction of the component of ε on K, we can use only the interferometric data.

5.3 Practical estimation

At this point, our procedure for reconstructing the inner surface of the DT-layer $R^* + \varepsilon(\theta, \varphi)$ is performed in two different steps:

- First, we reconstruct $\varepsilon_1(\rho^*, \theta), \varepsilon_2(\rho^*, \theta)$, (and eventually $\varepsilon_3(\rho^*, \theta)$, but, as we said above, this looks unnecessary, the approximation $\theta = \alpha$ from relations (10, 11) being sufficient in practice).

  Equivalently, we reconstruct $\varepsilon_1(\rho^*, \alpha)$, $\varepsilon_2(\rho^*, \alpha)$, $\varepsilon_3(\rho^*, \alpha)$, **that is we reconstruct 1) the intersection of the perturbed inner surface of the DT-layer with the plane corresponding to** ρ^*, **perpendicular to the optical axis, 2) the tangent planes to the inner surface along this curve. This is 3D information (our main contribution).**

- Second, we reconcile this information with the information obtained at the poles, by direct interferometry measurements.

Both steps are achieved by standard least square procedures.

- In the first step, the a-priori expansion (12) is used in restriction to (the plane) $\{\varphi = \varphi^*\}$: $\varepsilon(\theta, \varphi^*) = \sum_{i=1}^{i=k} \lambda_i . e_i(\theta, \varphi^*)$. As we said, we confuse this relation with the relation $\varepsilon(\alpha, \varphi^*) = \sum_{i=1}^{i=k} \lambda_i . e_i(\alpha, \varphi^*)$. Then, the practical measurements are the values $R_c(\alpha)$, that are considered equal to $R_c(\theta)$, and the main equation:

$$R_c(\alpha) \approx R^*(\rho^*) + a_1(\rho^*)\varepsilon_1(\rho^*, \alpha) + a_2(\rho^*)\varepsilon_2(\rho^*, \alpha),$$

from Theorem 8 gives rise to a set of linear equations, with unknown's the λ_i's, $i = 1, ..., k$.

The number of equations is the number of values of α taken into account. The corresponding values $R_c(\alpha)$ come from the method , described in section 3, to compute the inner part of the bright ring, corresponding to the caustic.

This overdimensionned system of linear equations is solved in the least-squares sense, and provides the curve [on the inner DT-layer, associated with the rays that intersect the caustic in the sensor plane] and the tangent planes to the inner surface along this curve.

-After that, we use this first information together with the direct measurements at the poles, and we reconcile both sets of data via a second standard least-squares step.

To finish, we show now some results of the full 3D reconstruction of the inner surface of the DT-layer. Up to now, contrarily to the results of Section 3 for the detection of the caustic, these are only simulation results, since we don't have yet the interferometric measurements at the poles.

The figure 11 shows a reconstructed inner surface of the DT-layer. For the same reconstruction, figure 12 shows the real surface compared to the reconstructed surface, along a horizontal and a vertical cut.

On this figure, the size ($R' = 10\,\mu$m) does not correspond to the practical size ($R^* \simeq 1.2\,$mm) of the microshell. The reason for this is just visualization. In other terms, **just in the drawing and not in the computations**, we have replaced the radius $R^* + \varepsilon$ by $R' + \varepsilon$, in order to magnify the perturbations.

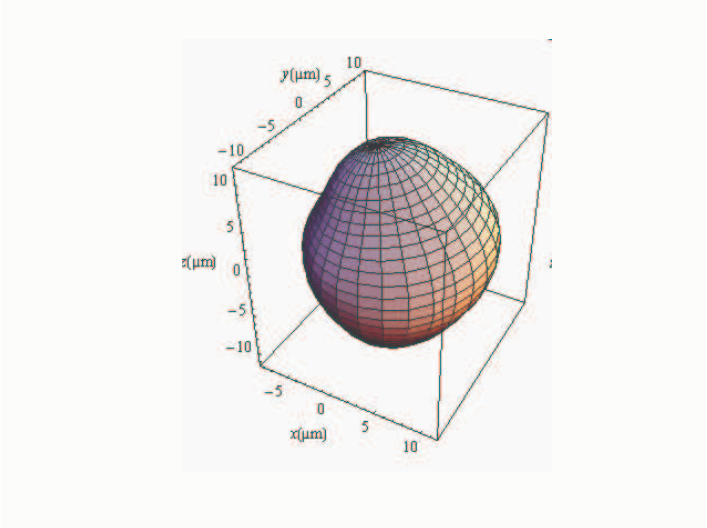

Figure 11: A reconstructed deformation

As required, the estimation errors are less than $1\,\mu$m.

6 CONCLUSION

In this paper, we have developed a general methodology to perform 3D reconstruction of an unknown surface $\mathcal{S}$ via shadowgraphic analysis. Our methodology is applied in the special case where the surface $\mathcal{S}$ is a small perturbation

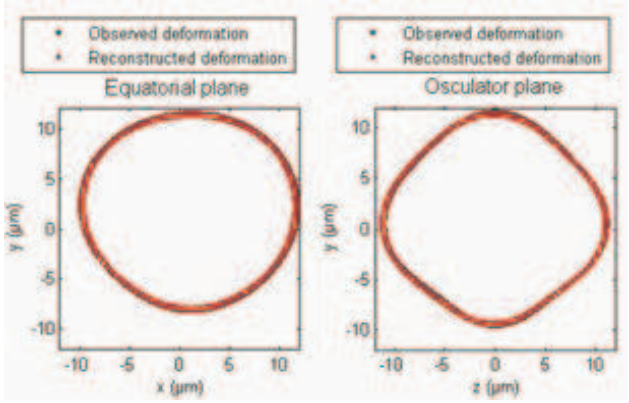

Figure 12: Comparison between cuts of original and reconstructed surfaces

$\mathcal{P}$ of a perfect sphere. However it could be extended to any situation which is a small perturbation $\mathcal{P}$ of some "ideal case".

A technique of "perturbation of singularities" allows to relate at **first order** the "caustic" of the system of optical paths to simultaneous information about both the surface and its tangent plane.

The **linearized** input-output mapping $\mathcal{R}$:

$$\text{surface } \mathcal{S} \times \text{tangent plane}^{\,7} \longrightarrow \text{caustic},$$

makes explicitly linear the inverse problem associated to 3D reconstruction.

We expand the unknown perturbation $\mathcal{P}$ in some adequate basis (spherical harmonics in our spherical case). Then we combine the relation $\mathcal{R}$ with extra data and/or other a-priori assumption to get a final linear system in terms of the coefficients of the expansion.

Finally this system is solved by using a classical least-squares method.

Our special case is the cryogenic target of the "laser mégajoule" project. It corresponds to rather complicated systems of optical paths, each of them producing a caustic.

Here, we use a single one, the most significant in terms of energy of optical paths. But it would be interesting (and this is certainly possible, since some of them have non negligible energy) to use also the caustics corresponding to other optical paths.

Moreover, in our situation we have very few information (a single series of caustics), corresponding to the unique direction of the incident system

[7] It would be mathematically more correct to consider, in place of this product, the so-called "tangent bundle" to the surface $\mathcal{S}$.

of collimated rays. This direction is unique due to the obstruction of the ambient space by the small cylindrical cavity containing the target. Then it is important to extract the maximum of information from this unique shadowgraphic picture.

Let us mention a very positive comparison (not presented in the paper) that has been made with other similar study developed at the University of Rochester ([3]). This different methodology simply assumes that the bright rings are perfect images of the "great circles" of the target. Hence this approach completely forgets the fact that the bright ring is a caustic and contains 3D information.

In this other study ([3]), the target is not located inside a cavity as in our case. Therefore a lot of shadowgraphic images are available. Of course, our methodology extends immediately to this case, just providing a number of relations of type $\mathcal{R}$, one for each of the shadowgraphic images.

Note also that this idea in ([3]) to consider the (ideal) bright rings as perfect images of the "great circle" of the DT surface, is a-priori a small mistake: our study in Section 2 shows that it is not the case, even in the unperturbed case.

Acknowledgement 11 *We gratefully acknowledge Pr. V. Zakalyukin, from the Lomonosov Moscow State University, for his intuition of Theorem 8, which is really crucial, since it makes the computations possible in practice. We also acknowledge Professor Seka and his group from Rochester University who were so kind to share with us the results of their experiments.*

References

[1] V.I. Arnold, A. Varchenko, and S. Goussein-Zadé. *Singularités des Applications Différentiables. I : Classification des Points Critiques, des Caustiques et des Fronts d'Onde.* (Editions Mir, Moscou, 1986).

[2] A. Choux, "Commande optimale d'un système de conformation cryogénique d'une couche solide d'isotopes de l'hydrogène dans un microballon par chauffage infra rouge", PhD thesis from University of Burgundy, to be defended December 2006.

[3] D.H. Edgell, W. Seka, R.S. Craxton, L.M. Elasky, D.R. Harding, R.L. Keck, L.D. Lund, and M.D. Wittman, "Characterization of cryogenic direct-drive ICF targets during studies and just prior to shot time", Fusion Science and Technology, **49** n°4, 616-625 (May 2006).

[4] F. Gillot, A. Choux, L. Jeannot, G. Pascal, P. Baclet, "Characterization of the DT layer of ICF targets by optical techniques", Fusion Science and Technology, **49** n°4, 626-634 (May 2006).

[5] H. Groemer, *Geometric applications of Fourier series and spherical harmonics*, (Cambridge University Press, 1996).

[6] S. Haan and al, "Update on Specifications for NIF Ignition Targets, and Their Rollup into an Error Budget", Fusion Science and Technology, **49** n°4, 553-557 (May 2006).

[7] E.W. Hobson, *The theory of spherical and ellipsoidal harmonics*, (New York : Chelsea, 1955).

[8] J. K. Hoffer, L. R. Foreman, "Radioactively Induced Sublimation in Solid Tritium", Physical Review Letters **60**, 1310-1313 (1988).

[9] J. D. Lindl, *Inertial Confinement Fusion*, (Springer, 1998).

[10] Marr, D. and Hildreth, E. "Theory of edge detection", Proc. R. Soc. Lond. B, **207**, 187-217 (1980).

[11] M. Martin, C. Gauvin, A. Choux, P. Baclet, G. Pascal, "The Cryogenic Target for Ignition on the LMJ: Useful Tools to Achieve Nominal Temperature and Roughness Conditions of the DT Solid Layer", Fusion Science and Technology, **49** n°4, 600-607 (May 2006).

[12] A. I. Nikitenko, S. M. Tolokonnikov, "Optical tomography of two layered targets: 3D parameters reconstruction from shadow image", To appear in Fusion Science and Technology

[13] V. Zakalyukin, "Applications of flag contact singularities", *New Developments in Singularity theory*, Nato series, Kluwer, 41-70 (2001).